Laser and Particle Beams (2010), *28*, 491–495.

doi:10.1017/S0263034610000480

Collisional and collisionless beam plasma instabilities

ANTOINE BRET
ETSI Industriales, Universidad de Castilla-La Mancha, Ciudad Real, Spain
(Received 8 June 2010; Accepted 10 June 2010)

Abstract

Collisions are a key issue regarding the instabilities involved in the fast ignition scenario for inertial confinement fusion. Because of the plasma density gradient through which the relativistic electron beam travels, unstable modes are collisionless at the beginning of the path, and collisional near the target core. While some works have been done on both regimes, the transition from the former to the later remains unclear. By implementing a hot fluid model accounting for a collisional return current, a theory is presented which bridges between the two regimes. The transition from one regime to the other is detailed in terms of the beam-to-plasma density ratio and the collision frequency. Purely collisional modes are found to arise at very low k, compared to the collisionless ones, and generate beam skin-depth size structures in accordance to previous works on resistive filamentation.

Keywords: Collisional beam plasma; Collisionless beam plasma; Fast ignition; Hot fluid model; Inertial confinement fusion; Relativistic electron beam

1. INTRODUCTION

The fast ignition scenario (FIS) for inertial confinement fusion (ICF) has prompted in recent years many theoretical (Tabak *et al.*, 2005), numerical and experimental works on relativistic beam plasma instabilities (Kodama *et al.*, 2001; Roth *et al.*, 2005; Honrubia *et al.*, 2004; Johzaki *et al.*, 2007). This approach to ICF consists in decoupling the pellet compression from its heating, relaxing the symmetry requirement, and the overall energy of the compression laser. The pellet is thus first compressed, and ignition then left to a relativistic electron beam (REB) generated by a petawatt laser shot on the pre-compressed target. If properly tailored, the REB deposits its energy at the pellet center, igniting the fuel. On its way from the border to the pellet core, the REB is compensated by an electronic return current from the background plasma, generating a two-stream configuration well-known for its instability. Due to the density gradient of the target (the center is about 10^4 denser than the border), the beam-plasma interaction is collisionless near the REB emitting region, and collisional near the center. Instabilities de-focus the beam, lowering the number of hot electrons eventually reaching the core. By exciting plasma waves, instabilities also transfer energy from the beam to the plasma. While such process is deleterious at the beginning of the beam path, it is welcome at the end where the beam is supposed to stop.

For the collisionless part, it has been established on the one hand that modes propagating perpendicularly (or obliquely) to the beam are the fastest growing ones for typical FIS parameters (Deutsch, 2004; Bret *et al.*, 2008). The beam is therefore broken-up into finite length filaments, which transverse typical size to the background plasma skin-depth $\lambda_p = c/\omega_p$. On the other hand, the unstable transport in the dense collisional region reveals a qualitatively different picture: the beam is still filamented, but the typical size of the filaments is now the *beam* skin-depth $\lambda_p = c/\omega_p$ (Gremillet *et al.*, 2002; Honrubia *et al.*, 2004). Within the FIS context, this means filaments is about 100 times larger than in the collisionless region. The question arises to pinpoint precisely the transition from one regime to another. Assessing this gap is important from the conceptual point of view, and mandatory to describe the beam propagation in the intermediate region.

Some recent work investigated this question for the FIS (Bret *et al.*, 2009). In particular, the influence of partial electronic plasma degeneracy near the pellet core was discarded, at least with respect to the unstable spectrum. Given the number of effect accounted for, this investigation was restricted to a single set of typical FIS parameters. As a consequence, the transition between the two regimes was not

Address correspondence and reprint requests to: Antoine Bret, ETSI Industriales, Universidad de Castilla-La Mancha, 13071 Ciudad Real, Spain. E-mail: antoineclaude.bret@uclm.es

documented in details. The goal of the present work is to fill this gap, through a simpler theoretical model highlighting the transition threshold in terms of the main variables. The first section is devoted to the formalism implemented. A detailed study of the transition, between the two regimes then follows, preceding the discussion and conclusion.

2. FORMALISM

We thus consider a relativistic beam of density n_b, velocity $\mathbf{v}_b$, and Lorentz factor $\gamma_b = (1 - v_b^2/c^2)^{-1/2}$ passing through a plasma of electronic density n_p. The plasma electrons are drifting with velocity $\mathbf{v}_p$ such as $n_b\mathbf{v}_b = n_p\mathbf{v}_p$ and the plasma ionic density n_i is such that $n_i = n_b + n_p$. The return current velocity $v_p = (n_b/n_p)v_p$ can be considered non-relativistic since we are not interested in the fully collisionless region where $n_b \sim n_p$. Collision-wise, the electrons from the beam are supposed to be collisionless due to their large velocity (Gremillet *et al.*, 2002). The terms collisional/collisionless rather refers to the background electrons. Their collisionality is here characterized by the plasma electron/ion collision frequency ν_{ei}.

Although the beam progresses in a density gradient, a Wentzel-Kramers-Brillouin like approximation where homogenous plasma calculations are applied locally, has been found valid for the FIS (Bret *et al.*, 2006).

The partial degeneracy of the core electrons is neglected, since it has been found that its role on the unstable spectrum is negligible. Finally, the orientation of the perturbation wave vector $\mathbf{k}$ needs to be arbitrary. While this is a source of significant analytical difficulties, such framework is necessary if one wishes to capture the most unstable mode (Bret *et al.*, 2005, 2007). As will be checked, the fastest growing modes in each regime are usually oblique. An investigation focusing on the filamentation instability with $\mathbf{k} \perp \mathbf{v}_b$, would thus render improperly the beam response by bypassing the most relevant modes in this respect.

After the background plasma ions, which are assumed at rest, electrons from the beam and the plasma share the same continuity equation,

$$\frac{\partial n_j}{\partial t} + \nabla \cdot (n_j \mathbf{v}_j) = 0, \tag{1}$$

where the subscript $j = b$ or p for the beam or the plasma. The Euler equation reads for the beam electrons,

$$\frac{\partial \mathbf{p}_b}{\partial t} + (\mathbf{v}_b \cdot \nabla)\mathbf{p}_b = -q\left(\mathbf{E} + \frac{\mathbf{v}_b \times \mathbf{B}}{c}\right) - \frac{\nabla P_b}{n_b}, \tag{2}$$

and for the plasma ones,

$$\frac{\partial \mathbf{v}_p}{\partial t} + (\mathbf{v}_p \cdot \nabla)\mathbf{v}_p = -\frac{q}{m}\left(\mathbf{E} + \frac{\mathbf{v}_p \times \mathbf{B}}{c}\right) - \nu\mathbf{v}_p - \frac{\nabla P_p}{n_p}. \tag{3}$$

The beam equation is thus collisionless and relativistic, while the plasma is non-relativistic and collisional. The pressure terms are expressed in terms of the temperatures through $\nabla P_j = 3k_B\, T_j\, \nabla\, n_j$, where k_B is the Boltzmann constant. Such an adiabatic treatment demands sub-relativistic temperatures, a requirement stronger for the beam than for the plasma (Siambis, 1979; Pegoraro & Porcelli, 1984). Though lengthy, the derivation of the dispersion equation is quite standard (Bret *et al.*, 2005) and eventually reads,

$$\det \mathcal{T} = 0, \tag{4}$$

where the tensor $\mathcal{T}$ is reported in Section 6, and expressed in terms of the dimensionless variables,

$$\alpha = \frac{n_b}{n_p},\ \mathbf{Z} = \frac{\mathbf{k}v_b}{\omega_p},\ \beta = \frac{v_b}{c},\ \tau = \frac{\nu}{\omega_p},\ \rho_j = \sqrt{\frac{3k_BT_j}{mv_b^2}}. \tag{5}$$

Calculations have been conducted aligning the beam velocity $\mathbf{v}_b$ with the z axis, and considering $\mathbf{k} = (k_x, 0, k_z)$. Components k_z and Z_z are therefore the parallel ones, while k_x and Z_x are the perpendicular ones.

3. THE COLLISIONAL/COLLISIONLESS TRANSITION

Figure 1 shows a typical growth-rate map arising from the numerical resolution of the dispersion equation. Modes localized around $Z_x \sim Z_z \sim 1$ are collisionless ones and produce filaments of transverse size $\sim c/\omega_p$. Note their oblique location, impossible to capture if restricting the exploration to the main axis. Unstable modes at small $\mathbf{Z}$ are collisional ones, as one can check they vanish when setting $\nu = 0$. The full spectrum is here clearly governed by these collisional modes. The fastest growing mode is found for

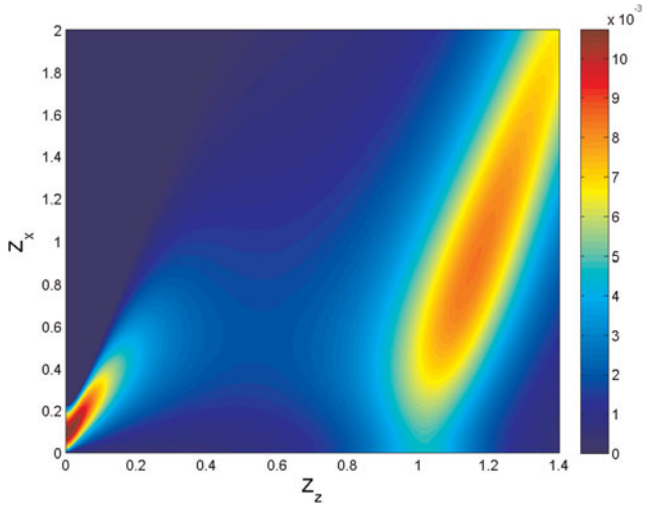

Fig. 1. (Color online) Typical growth-rate map in terms of (Z_x, Z_z). Parameters feature $\alpha = 10^{-2}$, $\rho_p = 4.2 \times 10^{-2}$, $\rho_p = 0.42$, $\tau = 0.3$, and $\gamma_b = 4$.

https://doi.org/10.1017/S0263034610000480 Published online by Cambridge University Press

$Z_z = 0.014$ and $Z_x = 0.11$, producing much larger filaments than the collisional modes. The simple relation between the beam and plasma skin-depths,

$$\lambda_b = \frac{\lambda_p}{\sqrt{\alpha}}, \tag{6}$$

shows that their size fits here the beam skin-depth, as expected when dealing with resistive filamentation (Gremillet *et al.*, 2002).

The unstable spectrum is thus clearly divided into two parts: the "lower" collisional spectrum, and the "upper" collisionless one. Our goal at this juncture is twofold: on the one hand, studying the evolution of the fastest growing mode (and its growth rate) of each part and on the other hand, documenting the transition between the two regimes. In view of the vast numbers of free parameters, we focus on the (τ, α) mapping, choosing for the other variables some FIS relevant values. We thus explore the parameters space,

$$\alpha \in [0,10^{-1}],\ \tau \in [0,0.5],\ \gamma_b = 4,$$
$$\rho_p = 4.2\times10^{-2}(T_p = 1\,\text{keV})\ \rho_b = 0.42(T_b = 100\,\text{keV}). \tag{7}$$

The fastest growing collisional mode $\mathbf{Z}_m$ and its growth rate have been calculated numerically over the parameters window specified above. Regardless of (τ, α), we find $\mathbf{Z}_m \sim (1,1)$ so that this part of the spectrum definitely generate skin-depth size structures. Figure 2 pictures the growth rate of these modes in terms of τ for $\alpha = 10^{-5}\ldots10^{-1}$. Regarding the alpha dependance, a α^{κ} with $\kappa \sim 1$ is retrieved, reminiscent of the exact kinetic scaling (Bret *et al.*, 2010).

Figure 3 now sketches the largest collisional growth rate in terms of (α, τ). We observe some quasi-constant τ and α scalings, which are numerically found very close to $\tau^{1/3}$ and $\alpha^{2/3}$.

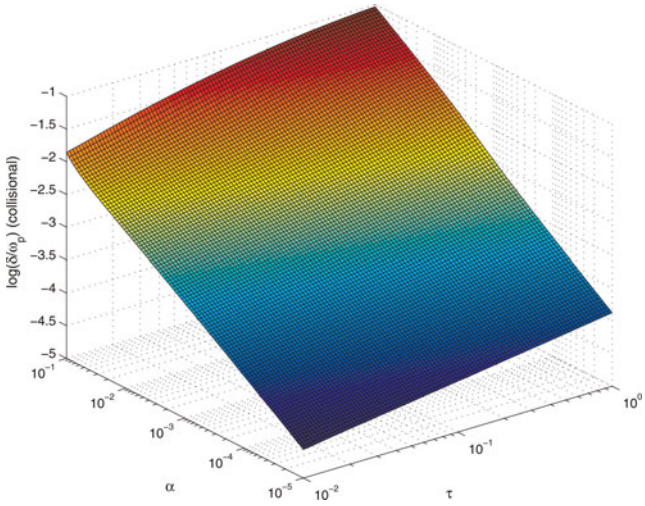

Fig. 3. (Color online) Growth-rate of the collisional modes (lower spectrum) in terms of τ and α.

The τ trends identified makes it clear that beyond a given collisionality threshold, collisional modes must surpass the collisionless ones. The resulting partition of the (τ,α) domain is pictured in Figure 4, where the beam trajectory from the pellet border to the core is superimposed. Instability wise, the beam clearly starts from the collisionless region to end up in the collisional one. The upper-spectrum is thus relevant at the beginning while the lower one is more important at the end.

Note that the collision parameter τ and the density ratio parameter α are not independent quantities. If restricting

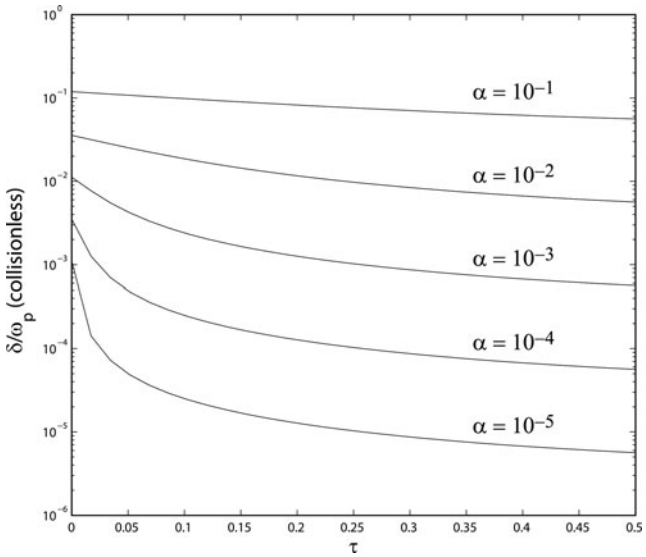

Fig. 2. Growth-rate of the collisionless modes (upper spectrum) in terms of τ for $\alpha = 10^{-5}\ldots10^{-1.}$

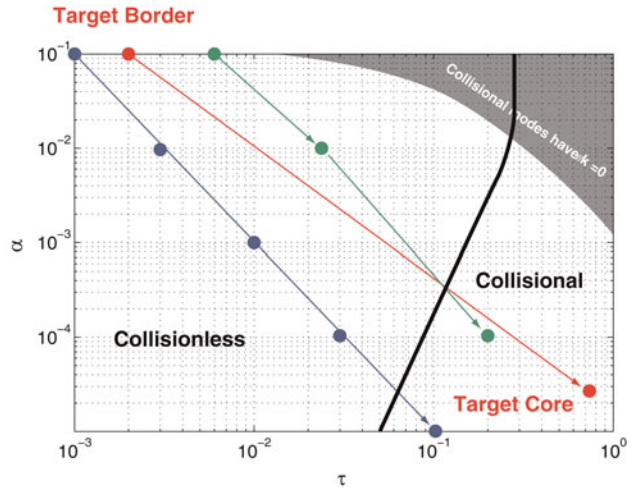

Fig. 4. (Color online) Portions of the (τ,α) plane governed by each kind of modes. The red path pictures the beam trajectory from the pellet border to the core. The blue path accounts for the relation between α and τ according to Eqs. (8) and (9). A more detailed analysis (Ren *et al.*, 2006) gives the green trajectory. In the upper-right corner domain, limited by the gray line, the fastest collisional modes have $k_{\|} = 0$.

https://doi.org/10.1017/S0263034610000480 Published online by Cambridge University Press

the former to electron-ion collisions, the collision frequency ν_{ei} reads (Huba, 2004),

$$\nu_{ei} = 2.91 \times 10^{-6} \frac{n_i(\mathrm{cm}^{-3})}{T_p^{3/2}(\mathrm{eV})} \ln \Lambda, \tag{8}$$

with

$$\ln \Lambda = 23.12 - \ln \left[\frac{n_p^{1/2}(\mathrm{cm}^{-3})}{T_p(\mathrm{eV})} \right]. \tag{9}$$

The beam path in the (τ, α) plane, as calculated according to the equations above and with $T_p = 1$ keV being pictured in blue in Figure 4. When accounting for a plasma temperature map extracted from a simulation of a pre-compressed target (Ren *et al.*, 2006), the path recovered is indicated in green. At any rate, the collisional regime is relevant near the core.

4. CHARACTERIZATION OF COLLISIONAL MODES

We finally turn to the most unstable wave-vector analysis. Our goal is mainly to check the size of the structures generated. To this extent, Figure 5 pictures the parallel (Z_z) and perpendicular (Z_x) components of the most unstable wave-vector. To start with, we find here another kind of transition: for most of the (τ, α) parameters, $\mathbf{Z}_m$ is oblique, that is, $Z_z \neq 0$. However, Z_z vanishes for $\tau > 0.5$ and $\alpha > 10^{-2}$ (the shape of the domain is more involved, as evidenced in Fig. 4), a regime that can be denoted as "resistive filamentation" since filamentation modes with $\mathbf{k} \perp \mathbf{v}_b$ are the fastest ones here. This region is represented in the upper-right corner of Figure 4.

The resistive filamentation regime is equally singled out on the perpendicular (Z_x) component with a specific scaling. Further numerical analysis shows that Z_x scales like $\alpha^{1/2}$ when $Z_z = 0$, and α^{σ} with $\sigma \sim 1/3$ otherwise. Interestingly, the $\alpha^{1/2}$ scaling is exactly what would be expected according to the *beam* skin-depth instead of the plasma one. In the oblique collisional regime, we still witness an increase of the filaments size when α decreases, but the scaling is too slow to keep up with the beam skin-depth.

5. CONCLUSION

A model of the REB transport in FIS context has been build to study the bridge between collisionless and collisional instabilities. Considering a relativistic, non-collisional diluted beam, passing through a non-relativistic and collisional return current, two kinds of unstable modes spontaneously arise from the resolution of the dispersion equation. For wave vectors $\mathbf{k}$ such as $k \sim \lambda_p$, collisionless unstable modes are triggered and generate plasma skin-depth size structures. At much lower k, collisional modes excited at finite collision frequency ν_{ei} generate *beam* skin-depth size structures. When ν_{ei} increases, collisionless instabilities are mitigated while collisional ones are boosted. As a result, a transition from one regime to the other occurs for a critical collision frequency. This threshold has been determined in terms of the beam-to-plasma density ratio, evidencing the collisional nature of the beam/target-core interaction.

Though the dielectric tensor and the dispersion equation are analytically known, it has not been possible so far to derive analytical expressions of the various quantities involved. Even when focusing on the filamentation modes with $\mathbf{k} \perp \mathbf{v}_b$, some approximations can yield a simpler dispersion equation, yet still analytically not extractable. The analytical derivation of the various scalings mentioned in this paper remains postponed for the future. Finally, a kinetic theory of the process would be interesting in order to confirm the collisionless/collisional transition and refine its description.

6. TENSOR ELEMENTS

The tensor $\mathcal{T}$ is symmetric and reads,

$$\mathcal{T} = \begin{pmatrix} \mathcal{T}_{11} & 0 & \mathcal{T}_{13} \\ 0 & \mathcal{T}_{22} & 0 \\ \mathcal{T}_{31} & 0 & \mathcal{T}_{33} \end{pmatrix}, \tag{10}$$

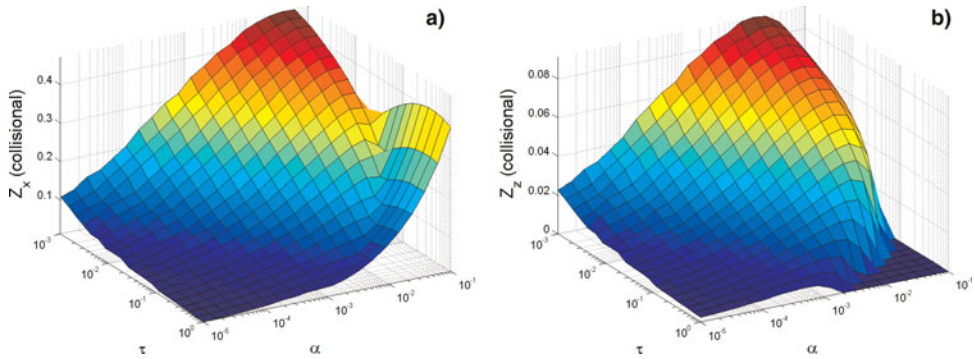

Fig. 5. (Color online) Perpendicular (Z_x, left) and parallel (Z_z, right) components of the most unstable wave-vector.

https://doi.org/10.1017/S0263034610000480 Published online by Cambridge University Press

where,

$$\mathcal{T}_{11} = x^2 - \frac{Z_z^2}{\beta^2} + \frac{-(x-Z_z)^2\alpha\gamma_b^3 + Z_z^2\alpha\rho_b^2}{(x-Z_z)^2\gamma_b^4 - \gamma_b(Z_z^2 + Z_x^2\gamma_b^2)\rho_b^2} - \frac{Z_z^2(x+Z_z\alpha)}{(Z_x^2+Z_z^2)(x+Z_z\alpha+i\tau)} + \frac{Z_x^2(x+Z_z\alpha)^2}{(Z_x^2+Z_z^2)\left(x^2+2xZ_z\alpha+Z_z^2\alpha^2 - Z_x^2\rho_p^2 - Z_z^2\rho_p^2 + i(x+Z_z\alpha)\tau\right)}, \quad (11)$$

$$\mathcal{T}_{22} = x^2 - \frac{Z_x^2+Z_z^2}{\beta^2} - \frac{\alpha}{\gamma_b} - \frac{x+Z_z\alpha}{x+Z_z\alpha+i\tau}, \quad (12)$$

$$\mathcal{T}_{33} = \frac{P}{\beta^2\gamma_b((x-Z_z)^2\gamma_b^3 - (Z_z^2+Z_x^2\gamma_b^2)\rho_b^2)} - \frac{Z_x^2(x+Z_z\alpha)}{(Z_x^2+Z_z^2)(x+Z_z\alpha+i\tau)} - \frac{(xZ_z - Z_x^2\alpha)^2}{(Z_x^2+Z_z^2)((x+Z_z\alpha)^2 - (Z_x^2+Z_z^2)\rho_p^2 + i(x+Z_z\alpha)\tau)}, \quad (13)$$

where,

$$P = 2xZ_x^2Z_z\gamma_b^4 + x^4\beta^2\gamma_b^4 - 2x^3Z_z\beta^2\gamma_b^4 + Z_x^2(-\gamma_b^3(\alpha\beta^2 + Z_z^2\gamma_b) + (\alpha\beta^2 + Z_z^2\gamma_b + Z_x^2\gamma_b^3)\rho_b^2) - x^2\gamma_b(Z_x^2\gamma_b^3 + \beta^2(\alpha + Z_x^2\gamma_b^2\rho_b^2 + Z_z^2(-\gamma_b^3 + \rho_b^2))), \quad (14)$$

and,

$$\mathcal{T}_{13} = \mathcal{T}_{31} = Z_x\frac{(x-Z_z)\gamma_b^3(-\alpha\beta^2 + (x-Z_z)Z_z\gamma_b) - Z_z(\alpha\beta^2 + Z_z^2\gamma_b + Z_x^2\gamma_b^3)\rho_b^2}{\beta^2((x-Z_z)^2\gamma_b^4 - \gamma_b(Z_z^2+Z_x^2\gamma_b^2)\rho_b^2)} + \frac{Z_xZ_z(x+Z_z\alpha)}{(Z_x^2+Z_z^2)(x+Z_z\alpha+i\tau)} + \frac{Z_x(-xZ_z + Z_x^2\alpha)(x+Z_z\alpha)}{(Z_x^2+Z_z^2)\left(x^2+2xZ_z\alpha+Z_z^2\alpha^2 - Z_x^2\rho_p^2 - Z_z^2\rho_p^2 + i(x+Z_z\alpha)\tau\right)}. \quad (15)$$

ACKNOWLEDGMENTS

This work has been achieved under projects ENE2009-09276 of the Spanish Ministerio de Educación y Ciencia and PAI08-0182-3162 of the Consejería de Educación y Ciencia de la Junta de Comunidades de Castilla-La Mancha.

REFERENCES

Bret, A., Firpo, M.-C. & Deutsch, C. (2006). Density gradient effects on beam plasma linear instabilities for fast ignition scenario. *Laser Part. Beams* **24**, 269.

Bret, A., Firpo, M.-C. & Deutsch, C. (2007). About the most unstable modes encountered in beam plasma interaction physics. *Laser Part. Beams* **25**, 117.

Bret, A., Firpo, M. & Deutsch, C. (2005). Bridging the gap between two stream and filamentation instabilities. *Laser Part. Beams* **23**, 375.

Bret, A., Gremillet, L. & Bénisti, D. (2010). Exact relativistic kinetic theory of the full unstable spectrum of an electron-beam-plasma system with maxwell-jüttner distribution functions. *Phys. Rev. E* **81**, 036402.

Bret, A., Gremillet, L., Bénisti, D. & Lefebvre, E. (2008). Exact relativistic kinetic theory of an electron-beam-plasma system: Hierarchy of the competing modes in the system-parameter space. *Phys. Rev. Lett.* **100**, 205008.

Bret, A., Marín Fernández, F.J. & Anfray, J.M. (2009). Unstable spectrum of a relativistic electron beam interacting with a quantum collisional plasma: application to the fast ignition scenario. *Plasma Phys. Contr. Fusion* **51**, 075011.

Deutsch, C. (2004). Penetration of intense charged particle beams in the outer layers of precompressed thermonuclear fuels. *Laser Part. Beams* **22**, 115.

Gremillet, L., Bonnaud, G. & Amiranoff, F. (2002). Filamented transport of laser-generated relativistic electrons penetrating a solid target. *Phys. Plasmas* **9**, 941.

Honrubia, J., Antonicci, A. & Moreno, D. (2004). Hybrid simulations of fast electron transport in conducting media. *Laser Part. Beams* **22**, 129.

Huba, J.D. (2004). *NRL Plasma Formulary*. Washington, DC: Naval Research Laboratory.

Johzaki, T., Sakagami, H., Nagatomo, H. & Mima, K. (2007). Holistic simulation for FIREX project with FI3. *Laser Part. Beams* **25**, 621

Kodama, R., Norreys, P.A., Mima, K., Dangor, A.E., Evans, R.G., Fujita, H., Kitagawa, Y., Krushelnick, K., Miyakoshi, T., Miyanaga, N., Norimatsu, T., Rose, S.J., Shozaki, T., Shigemori, K., Sunahara, A., Tampo, M., Tanaka, K.A., Toyama, Y., Yamanaka, Y. & Zepf, M. (2001). Fast heating of ultrahigh-density plasma as a step towards laser fusion ignition. *Nat.* **412**, 798.

Pegoraro, F. & Porcelli, F. (1984). Equation of state for relativistic plasma waves. *Phys. Fluids* **27**, 1665.

Ren, C., Tzoufras, M., Tonge, J., Mori, W.B., Tsung, F.S., Fiore, M., Fonseca, R.A., Silva, L.O., Adam, J.-C. & Heron, A. (2006). A global simulation for laser-driven mev electrons in 50- mu m-diameter fast ignition targets. *Phys. Plasmas* **13**, 056308.

Roth, M., Brambrink, E., Audebert, P., Blazevic, A., Clarke, R., Cobble, J., Cowan, T., Fernandez, J., Fuchs, J., Geissel, M., Habs, D., Hegelich, M., Karsch, S., Ledingham, K., Neely, D., Ruhl, H., Schlegel, T. & Schreiber, J. (2005). Laser accelerated ions and electron transport in ultra-intense laser matter interaction. *Laser Part. Beams* **23**, 95.

Siambis, J. G. (1979). Adiabatic equations of state for intense relativistic particle beams. *Phys. Fluids* **22**, 1372.

Tabak, M., Clark, D.S., Hatchett, S.P., Key, M.H., Lasinski, B.F., Snavely, R.A., Wilks, S.C., Town, R.P.J., Stephens, R., Campbell, E.M., Kodama, R., Mima, K., Tanaka, K.A., Atzeni, S. & Freeman, R. (2005). Review of progress in fast ignition. *Phys. Plasmas* **12**, 057305.